

APPLICATION OF THE FLUX BENDING EFFECT IN AN ACTIVE FLUX-GUIDE FOR LOW-NOISE PLANAR VECTOR TMR MAGNETIC SENSORS

Luong Van Su^{1, 2, 3, *}, Nguyen Anh Tuan^{1, *}, Nguyen Anh Tue⁴, Nguyen Tuyet Nga⁴,
Hoang Quoc Khanh¹, Nguyen Ngoc Lan¹, Nguyen Tuan Anh⁵

¹International Training Institute for Materials Science (ITIMS), Ha Noi University of Science and Technology (HUST), Dai Co Viet, Hai Ba Trung, Ha Noi

²Faculty of Electrical and Electronic Engineering, Phenikaa Institute for Advanced Study (PIAS), Phenikaa University, Ha Noi

³Phenikaa Research and Technology Institute (PRATI), A&A Green Phoenix Group, 167 Hoang Ngan, Ha Noi

⁴Institute of Engineering Physics (IEP), Ha Noi University of Science and Technology (HUST), Dai Co Viet, Hai Ba Trung, Ha Noi

⁵Hanoi Community College (HCC), Trung Kinh, Cau Giay, Ha Noi

*Email: natuan.itims@hust.edu.vn and su.luongvan@phenikaa-uni.edu.vn

Received: 8 June 2018; Accepted for publication: 15 November 2018

ABSTRACT

A concept of a planar vector magnetic sensor comprising in-plane tunnel magnetoresistive (TMR) sensors and an active flux-guide (AFG) was introduced in this work. The AFG redirected the magnetic flux at high-frequency benefiting a vertical detection capability and suppressing the field noise of the TMR at low-frequency measurement. The vertical sensitivity of 19.5 V/T was close to the in-plane sensitivity of 19.2 V/T. In addition, the 1-Hz field noise was suppressed from 6 nT/ $\sqrt{\text{Hz}}$ down to 0.4 nT/ $\sqrt{\text{Hz}}$. The flux bending effect of the AFG was also verified by the angular measurements with the angular deflection was found to be about 50°. It revealed that the vertical field component was certainly detected by the in-plane sensor, and the proposed method was a feasible approach for the development of the low-noise planar vector magnetic sensor.

Keywords: low-frequency noise; magnetometers, magnetic fields; modulation technique; TMR

Classification numbers: 2.2.1; 2.10.1; 4.4.1.

1. INTRODUCTION

Tunneling magnetoresistance sensors (TMR) were widely used in the magnetic sensing applications by its advantages of high magnetoresistance ratio, low cost and low power consumption [1, 2], e.g. current measurement, electronic compass, automation, and geomagnetic applications [3]. To expand the applications of the magnetic sensors, the high-performance magnetic sensor should be developed, including the miniature, the co-planarization, the multi-axis vector sensors and so on. In the past decade, many research groups developed the vector magnetometers using the solid-state sensors [4, 5] owing to its advantages, including the CMOS compatibility of TMR so that the devices have been easily integrated. Excluding the traditional three-axis design that used three sensors for three axes, in which three sensors were aligned respectively their sensing directions along three vectors of the Cartesian coordinate system [6]. Whereas, the flux-guide technique was proposed in recent years to construct a vector magnetometer using co-planar sensors [4, 5]. In fact, flux-guide helps to induce the in-plane magnetic field component, which can be measured by an in-plane sensor. However, the drawbacks of the flux-guide are hysteresis of its materials and there is no contribution to improving the noise of the incorporated sensors. Although, the detectivity of the TMR sensor has been known on the order of pico-tesla (pT) [7], and noise spectral density was less than 1 nT/ $\sqrt{\text{Hz}}$ at several of kilohertz [8]. Unfortunately, the resolution of TMR sensors in low field measuring applications was severely restricted by the low-frequency ($1/f$) noise. Many efforts to suppressing $1/f$ noise have been reported, e.g. the micro-electro-mechanical-system (MEMs) flux concentrators (FC) [9, 10] and modulated flux densities [11]. The modulation technique said that the hysteresis of a magnetic sensor incorporated with a soft magnetic FC could be eliminated by modulating the permeability of the FC played as an active flux-guide (AFG) [12]. In our previous work proved that the $1/f$ noise of a TMR was improved by a factor of 12 and the noise level at 1-Hz was about 0.33 nT/ $\sqrt{\text{Hz}}$ @1Hz using a shielding chopper [13].

In this work, we present a concept of a vector magnetic sensor comprising a square hollow AFG, so that a TMR sensor was aligned at the position where flux was redirected nearby the outer edge of the AFG. Therefore, the vertical field component (B_z) would be redirected becoming an in-plane magnetic field component, which easily caught by a planar sensor. The working principle of AFG can be interpreted as follows. Normally, with only tubular Metglas core, its function likes a passive flux-guide, which induced the in-plane field components. Besides, the flux density nearby sensor is concentrated leading to boosting the sensitivity of the sensors. In this design, the permeability of the core material was oscillated leading to the core being switched from the unsaturated to the saturated states. It means that the flux densities around the sensor were modulated at high frequency, which helps to move the operating point of the TMR sensor to the high-frequency regime, where there is the only white noise level. Thus, the $1/f$ noise of the TMR sensor is suppressed. The AFG is not only contributed to suppressing $1/f$ noise but also a promising method to develop a vector magnetometer for sensing geomagnetic field using planar TMR sensors. The sensitivity, angular responses, and noise characteristic of the engineered sensor were realized and verified. The experimental results are presented.

2. EXPERIMENTAL

The concept of a planar TMR sensor for the vertical detection with an AFG is shown in Fig.1. The TMR sensor used in this work was the commercial TMR2102 sensor provided by MDT Inc. [14]. The sensor has the inner structure consisting of four active TMR arrays formed in a full Wheatstone bridge. Each TMR array was circuited in series of the hundreds of magnetic

tunnel junction (MTJ). The sensor's nonlinearity is below 1% in the range of ± 30 Oe. The intrinsic sensitivity of the sensor is 4.9 mV/V/Oe within the linear range [14]. The AFG constructed by a soft magnetic core and an excitation coil. The AFG was designed in a square hollow shape, which was 14 mm in length and 7 mm of the square edge. In our previous design [13], the cylindrical chopper was used. However, the edge of Metglas core hardly bends in a perfect circle leading to the distribution of the flux density being uniform. Hence, this design with a square shape, the edge of the metglas was a line. It helps easily to form the shaped tube and the flux distribution is more uniform. The core's material is the Metglas-2714A, from Metglas Inc. [15]. The thickness is about 0.6 mil (~ 15 μm). The metglas is easily saturated with an external magnetic field below 0.1 Oe [15]. The single core of the AFG was wrapped with copper wires to modulating the permeability of the Metglas. The number of turns of the excitation coil was about 100, which induced a magnetizing field of 0.2 Gauss for the modulation. The wiring configuration of the AFG is shown in Fig. 1. Fig. 1(a) shows the complete isometric view of the AFG design, while Fig. 1(b) show the sectional top view of the AFG, including the metglas core and copper wires. Figs. 1(c) and (d) show the sectional side view of the AFG in the simulation. In order to simply show the bending effect of the AFG, the cutting side of the AFG was chosen in the 2D simulation so that two sides of the AFG tube are illustrated by two slide bars. The simulation was carried out using Maxwell V16.0 simulator to show the bending effect of the AFG [16]. The TMR sensor was placed at the position nearby the outer edge of the chopper tube, where the in-plane magnetic field component induced by the AFG could be detected, as illustrated in Fig 1(d). In Figs. 1(c) and (d), only applied field was shown, while the magnetizing field induced by excitation coil was not. When the magnetizing field is ON (current ON), it magnetizes the metglas core so that the permeability is low leading to the applied magnetic field is homogeneous, as shown in Fig. 1(c). Whereas, when current is OFF the core is demagnetized so that the core has an extremely high permeability making the flux density being concentrated, which was so called "bending effect", as shown in Fig. 1(d). The optimal position of the TMR with a flux-guide has also been reported by the author in previous work [12, 13, 17]. The sensor must be placed as close as possible to the outer edge of the chopper tube. The flux bending effect of an AFG could be estimated by the function between the sensitivity and the excitation current. Fig. 2 shows the bending effect of the AFG with DC current passing the excitation coil. TMR sensor was biased by a 3.5 V DC voltage. The effective sensitivity changed from 109 V/T to 38 V/T with the current changing from 0 A to 0.4 A, respectively. Due to the trade-off between the power consumption and the effective sensitivity, and the sensitivity was slightly reduced from 0.2 to 0.4 A of DC current so that the amplitude of the excitation current has been set at 0.2 A of a square wave. The square wave excitation signal was set about 1 kHz that far enough from the $1/f$ corner. The excitation signal was generated by an Oscillator 2 MHz and divided by a binary divider (CD4020). The output of the sensor was amplified via an instrumentation amplifier (INA129), and a lock-in amplifier using a mixer of AD630. An active low-pass filter (LPF) with a cutoff frequency of 10 Hz was used to narrow the bandwidth for further suppressing noise and retrieving the dc signal that is proportional to the measuring magnetic field.

The sensitivity of the sensor was determined by taking the slope between the referenced magnetic field and the response output of the TMR sensor. The reference magnetic field was generated by a Helmholtz coil with the sweeping frequency of 0.5 Hz and amplitude of ± 60 μT . The sweeping signal was generated by a multifunction synthesizer (HP-8904A). The applied field orientations were installed in three cases: $U_x(B_x)$, $U_x(B_y)$, and $U_x(B_z)$. The sweeping fields and the demodulated output were recorded by a data acquisition device (NI-MyDAQ) from the National Instruments. To analyze the noise spectral densities, the sensor was shielded by a tri-

layer magnetic shielding to set zero fields around TMR sensor for preventing the interference from the magnetic fields induced by the electrical equipment. The shielding chamber was made by Mu-metal with an extremely high permeability (> 100000). The thickness of the Mu-metal was about 1 mm. The dimension of the chamber was designed in 500 mm high and a diameter of 200 mm. The space between each layer was about 20 mm. The TMR sensor with AFG was placed at the center of the shielding chamber and three caps of the shielding chamber were also made by Mu-metal. A spectrum analyzer, HP-3582A, was used to record the noise signal. The responses of the sensor to each external magnetic field were measured the peak-to-peak output of the sensor when the TMR sensor was manually being rotated in the tri-axis sweeping fields of the B_x , B_y , and B_z of the three-dimensional Helmholtz coils and their strength was about $\pm 60 \mu\text{T}$.

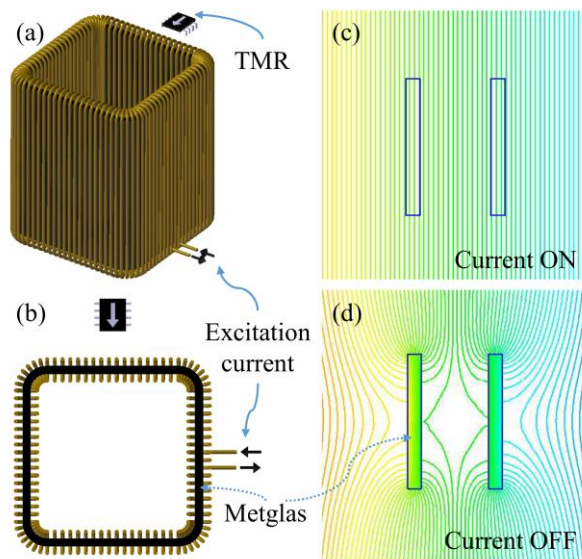


Figure 1. Structure of the AFG: (a) isometric view, (b) sectional top view, (c) 2D simulation of the flux bending effect with excitation current ON, and (d) current OFF.

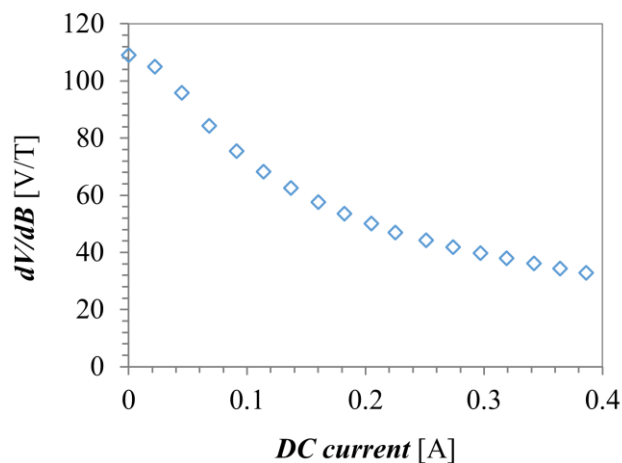


Figure 2. Flux bending effect as a function of DC current passing the excitation coil.

3. RESULTS AND DISCUSSION

3.1. The sensitivities of the TMR sensor with and without an AFG

Table 1 shows the sensitivities of the sensor with and without of the AFG. In the case of no AFG, the applied field was set up in parallel to the normal sensing direction of the sensor, $U_x(B_x)$, the obtained sensitivity was 165 V/T. Whereas in the case of the external field was applied along the z -axis, $U_x(B_z)$, an obtained low sensitivity was about 1.3 V/T. It indicated that the TMR sensor was nearly insensitive to the vertical magnetic field. A low vertical sensitivity may be caused by the cross-detection error. In the case of the AFG, the sensitivity of the sensor was 19.2 V/T, which was resulted by the modulated efficiency. When incorporating the sensor with an AFG, the exposed magnetic field was bent from out-of-plane to the normal sensing direction of TMR, $U_x(B_z)$, the sensitivity of the sensor was about 19.5 V/T and the maximum sensitivity of 21 V/T at the 50° from the normal sensing direction of the TMR, where was the angle between the x -axis and the z -axis. The obtained results revealed that the benefit of AFG to redirect the flux line from the vertical component to the horizontal component, which can be caught easily by a planar TMR sensor.

Table 1. Horizontal and vertical sensitivities of the TMR sensor with and without an AFG.

dV/dB (V/T)				
Without AFG		With AFG		
$U_x(B_x)$	$U_x(B_z)$	$U_x(B_x)$	$U_x(B_z)$	$U_x@(\angle 50^\circ x-z)(B_z)$
165	1.3	19.2	19.5	21

3.2. The outputs of TMR sensor response to the applied magnetic fields

The responses of the TMR sensor with and without of the AFG to each B_x , B_y and, B_z components were carried out. The system was placed on an accurate rotation stage for verifying the angular response to the three sweeping magnetic fields, as shown in Figs. 3(a, b) and 4(a, b). The sensor was rotated manually in a completed 360° with the interval of 10° . The first, the TMR sensor was rotated about the square hollow axis of the AFG, i. e. along the z -axis (B_z). After that sensor was rotated about the y -axis (B_y) to verify the bending effect of the AFG. The experiments were set up with both cases of the TMR sensor without and with an AFG for comparison.

3.2.1. Rotation system about the vertical axis of the sensor

Figure 3 shows the setup and the output of TMR sensor rotating about the axis of the square hollow AFG in the reference magnetic fields in both cases of without (Fig. 3.a) and with the AFG (Fig. 3.b). The output of the TMR sensor without AFG was about ± 2 V smaller than that in the case of the TMR incorporated AFG was ± 6 V. The results were caused by the fact that we only focused on the bending flux so that we kept the small gain of 50 in the bare TMR case, and increased the TMR incorporated with AFG high enough, which was about 2350, for showing clearly response of the measurement. The angular responses (U_x) to the B_x and B_y were differed by 90° , revealing that the referenced magnetic fields were pretty orthogonal. Additionally, the output ($U_x(B_z)$) of the bare TMR sensor (without AFG) was only 0.1 V, it seems to be the almost insensitive state to the B_z of the sensor. Whereas, with AFG, the output of the sensor was

constant at 7 V with the vertical magnetic field (B_z). It confirmed again that the vertical field component could be caught by a planar sensor owing to the bending effect of the AFG.

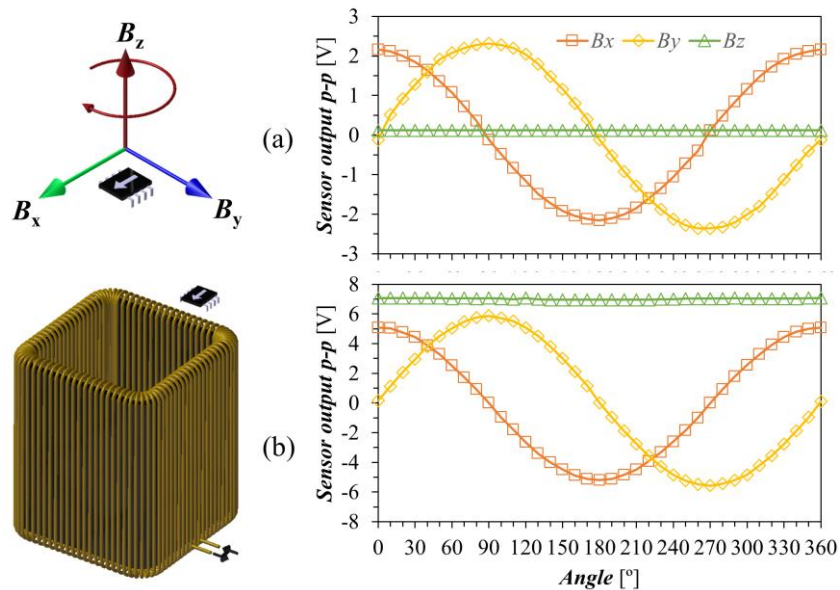


Figure 3. Rotating system about the z-axis of the AFG: (a) single TMR, and (b) TMR incorporated with the AFG.

3.2.2. Rotation system about the y-axis

The angular bending effect could be figured out by the results of the rotating system about the y-axis. Interestingly, the responses of the TMR sensor in both case without and with the AFG were shifted by an angle of 50° . It indicated that the flux lines were bent by an angle that formed by the B_z to the normal sensing direction of the TMR. The result was also consistent with the output of TMR could be reached a maximum of 8 V@ 50° (Fig. 4b). Whereas, in the without AFG case, the maximum of the TMR's output was reached a maximum value of 2 V@ 90° (Fig.4a). In Fig. 4b, the output of TMR at 50° was higher than that in the case of the TMR incorporated AFG and rotating sensor about z-axis by 90° , as shown in Fig. 3b, which could be interpreted by fact that the sensitivity of the TMR sensor at 50° was higher, as mentioned in Table 1. The response of the TMR sensor to the B_y field component was almost constant owing to the external field was always vertically to the sensing axis of the TMR. Additionally, the other field components, B_x and B_z , were observed sinusoidally between ± 8 V. The obtained sinusoidal responses of the TMR incorporated AFG revealed that due to the flux density about the sensor was switched between the saturated state to the saturated state of the Metglas core. The bending effect was active at the unsaturated state of the core, and the magnetizing field induced by the excitation coil is enough to magnetize and demagnetize the core. The bending effect is active in the unsaturation state so that the demagnetization of the core is dominant. Therefore, the response of the sensor incorporated AFG is only depended on the aspect ratio (the aspect ratio is 2 in this work and it is small enough) [17]. The AFG plays as a flux guide. Thus, flux density was also responded like the without an AFG case in a completed rotation of 360° .

3.3. Impact of the AFG on the 1/f noise

The spectral densities of the field noises of TMR sensor with and without the AFG are shown in Fig. 5. The intrinsic noise of the sensor was presented for evaluating the performance in the reducing $1/f$ noise by the reduction ratio, which was determined by taking the division between the TMR's noise without and with the AFG. The intrinsic noise of the bare TMR sensor was about $6 \text{ nT}/\sqrt{\text{Hz}}@1\text{Hz}$, and there was a small slope from 0.1-Hz to 10 Hz. According to the datasheet of the TMR, the 1-Hz noise could be higher ($10 \text{ nT}/\sqrt{\text{Hz}}@1\text{Hz}$). With AFG, the noise spectrum was nearly flat within the frequency span recording. The $1/f$ knee was shifted to below 0.1-Hz. The minimum noise level of TMR sensor was reached to $0.4 \text{ nT}/\sqrt{\text{Hz}}@1\text{Hz}$. The noise reduction could be interpreted by the benefit of the phase sensitive detection (PSD) technique in this work. With the PSD technique, the measured signal (applied magnetic field) is extracted from the modulated signal. Besides, only the signals having the angular frequencies close to the excitation frequency will be passed through the PSD system (1 kHz in this work). Furthermore, the other components, which are approximate to the excitation frequency will be further filtered via an LPF. Therefore, the noise was suppressed certainly by the chopping technique using an AFG.

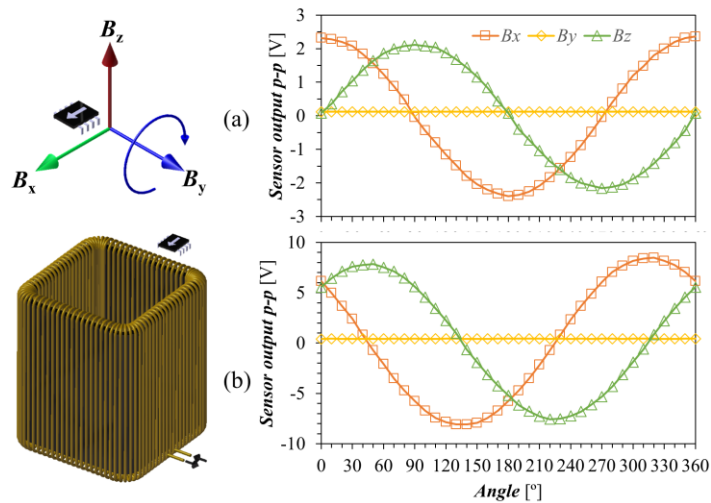


Figure 4. Rotating system about the y-axis of the AFG: (a) single TMR, and (b) TMR incorporated with the AFG.

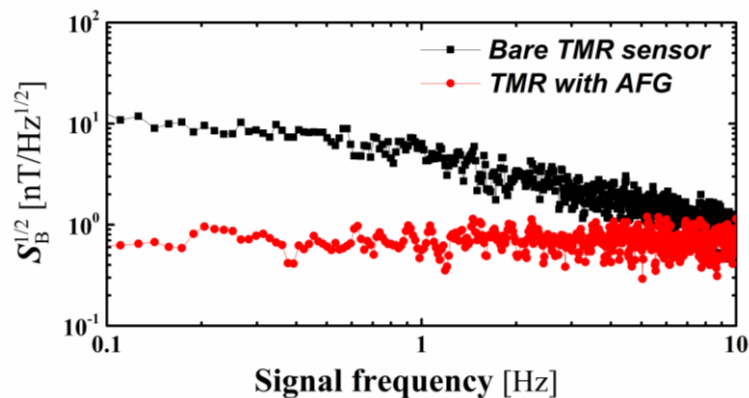


Figure 5. The noise of the TMR sensor with and without the AFG.

4. CONCLUSIONS

We have shown the development and experimental validation of a low noise TMR sensor incorporated with an AFG for the concept of a planar vector magnetic sensor. The bending effect and lessening noise performance were proved in the AFG. One hand, AFG deflected the flux lines from out-of-plane to inducing the horizontal field components that could be sensed easily by the planar sensors. On the other hand, AFG enhanced the sensitivity of the incorporated sensor. Importantly, with the modulation flux density, the working point of the TMR was moved to the high-frequency regime, where there was not $1/f$ field noise. The field noise could be observed of $0.4 \text{ nT}/\sqrt{\text{Hz}}@1\text{Hz}$. The proposed concept of the vector magnetometer system can be used to develop a low noise three-dimensional magnetic field sensor using co-planar TMR sensors. Due to the bending angle between the vertical axis and horizontal axis was about 50° and the unavoidable misalignment of the sensors leading to three axes would certainly be not orthogonal so that a calibration process is needed.

Acknowledgments. This research is funded by the Vietnam National Foundation for Science and Technology Development (NAFOSTED) under the grant number 103.02-2016.03.

REFERENCES

1. Freitas P. P., Ferreira R., Cardoso S. - Spintronic Sensors, Proc. IEEE **104** (2016) 1894-1918.
2. Ripka P., Závěta K. - Chapter 3 Magnetic Sensors: Principles and Applications, Handbook of Magnetic Materials **18** (2009) 347-420.
3. Robbes D. - Highly sensitive magnetometers—a review, Sens. Actuators, A Phys. **129** (2006) 86-93.
4. Schott C., Racz R., Manco A., Simonne N. - CMOS Single-Chip Electronic Compass With Microcontroller, IEEE Journal of Solid-State Circuits **42** (2007) 2923-2933.
5. Jeng J. T., Chiang C. Y., Chang C.H., Lu C. C. - Vector Magnetometer with Dual-Bridge GMR Sensors, IEEE Trans. Magn. **50** (2014) 1-4.
6. Luong V. S., Jeng J. T., Lu C. C., Hsu H. Y. - Low-noise tunneling-magnetoresistance vector magnetometers with flux chopping technique, Measurement **109** (2017) 297-303.
7. Ingvarsson S., Xiao G., Parkin S.S.P., Gallagher W. J., Grinstein G., Koch R. H. - Low-Frequency Magnetic Noise in Micron-Scale Magnetic Tunnel Junctions, Phys. Rev. Lett. **85** (2000) 3289-3292.
8. Stutzke N.A., Russek S. E., Pappas D. P., Tondra M. - Low-frequency noise measurements on commercial magnetoresistive magnetic field sensors, J. Appl. Phys. **97** (2005) 10Q107.
9. Edelstein A. S., Fischer G. A., Pedersen M., Nowak E. R., Cheng S. F., Nordman C. A. - Progress toward a thousandfold reduction in $1/f$ noise in magnetic sensors using an ac microelectromechanical system flux concentrator (invited), J. Appl. Phys. **99** (2006) 08B317.
10. Edelstein A. S., Burnette J. E., Fischer G. A., Olver K. W.E. Jr., Nowak E., Cheng S. F. - Validation of the microelectromechanical system flux concentrator concept for minimizing the effect of $1/f$ noise, J. Appl. Phys. **105** (2009) 07E720.

11. Jander A., Nordman C. A., Pohm A. V., Anderson J. M. - Chopping techniques for low-frequency nanotesla spin-dependent tunneling field sensors, *J. Appl. Phys.* **93** (2003) 8382-8384.
12. Su V. L., Jeng J. T., Hsu J. H., Chang C. R., Lu C. C. - Tunneling-Magnetoresistance Vector Magnetometer with Deflection Flux-Chopper, *IEEE Trans. Magn.* **52** (2016) 1-4.
13. Luong V. S., Chang C. H., Jeng J. T., Lu C. C., Hsu J. H., Chang C. R. - Reduction of Low-Frequency Noise in Tunneling-Magnetoresistance Sensors with a Modulated Magnetic Shielding, *IEEE Trans. Magn.* **50** (2014) 1-4.
14. MultiDimension Technology Co. Ltd, TMR2102 linear sensor, available online: <http://www.dowaytech.com/en/1394.html>. accessed date: September 24, 2018
15. Metglas. Inc., Metglas-2714A. available online: http://www.metglas.com/products/magnetic_materials/2714a.asp, accessed date: September 24, 2018
16. ANSYS Maxwell, available online: <http://www.ansys.com/products/electronics/ansys-maxwell>, accessed date: September 24, 2018
17. Luong V. S., Su Y. H., Lu C. C., Jeng J. T., Hsu J. H., Liao M. H., Wu J. C., Lai M. H., Chang C. R. - Planarization, Fabrication and Characterization of Three-dimensional Magnetic Field Sensors, *IEEE Trans. Nanotechnol.* **17** (2018) 11-25.